ELSEVIER

Biochimica et Biophysica Acta 1319 (1997) 119–132

BIOCHIMICA ET BIOPHYSICA ACTA
BBA

Rebinding of the extrinsic proteins of Photosystem II studied by electron microscopy and single particle alignment: an assessment with small two-dimensional ordered arrays of Photosystem II

Mark F. Rosenberg [a,*], Andreas Holzenburg [b,c], Fiona H. Shepherd [b,1], William V. Nicholson [a,2], Toby D. Flint [b], Robert C. Ford [a]

[a] *Department of Biochemistry and Applied Molecular Biology, UMIST, PO Box 88, Manchester, M60 1QD, UK*
[b] *Department of Biochemistry and Molecular Biology, University of Leeds, Leeds, LS2 9JT, UK*
[c] *Department of Biology, University of Leeds, Leeds, LS2 9JT, UK*

Received 19 March 1996; revised 27 September 1996; accepted 7 October 1996

Abstract

Structural analysis of weakly ordered two-dimensional (2-D) ordered arrays of Photosystem II (a photosynthetic membrane protein complex) has been carried out using single-particle alignment and averaging (SPA). Although this averaging technique is normally applied to randomly oriented solubilised particles, we have found that it is also highly effective for the analysis of membrane-located 2-D ordered arrays and that the arrays can be used to check the effectiveness of the rotational alignment routines. Successful rotational alignment varied in the range 75 to 66% and 26 to 19%, depending on the stain used and hence the signal-to-noise ratio, and the data were used to address questions of space group assignments for Photosystem II 2-D ordered arrays. We thus hoped to settle the controversy as to the oligomeric form of PS II in native thylakoids, i.e., the monomeric vs. dimeric model. The methods were applied to the study of the removal and rebinding of extrinsic subunits in Photosystem II. Information on the location of the subunits in this large membrane protein complex is presented here.

Keywords: Photosystem II; Rebinding; Extrinsic protein; Electron microscopy; Single-particle alignment

Abbreviations: DMAB, borane-dimethylamine complex; DMBQ, dimethylbenzoquinone; EM, electron microscope; LHCP, (LHCII) light-harvesting complex; OEC, oxygen-evolving complex; PS II, Photosystem II; SDS-PAGE, sodium dodecyl sulfate-polyacrylamide gel electrophoresis; STEM, scanning transmission electron microscope; TEM, transmission electron microscope; 2-D, two-dimensional

* Corresponding author. Fax: +44 161 2360409. E-mail: mark.rosenberg@umist.ac.uk
[1] Present address: Institute for Cardiovascular Research, Research School of Medicine, University of Leeds, LS2 9JT, UK.
[2] Present address: Department of Chemistry, University of Glasgow, Glasgow, G12 8QQ, UK.

PII S0005-2728(96)00124-7

1. Introduction

Electron microscopy (EM) has the potential to provide high resolution (< 0.4 nm) data for the structure of biological molecules [1,2]. However, the low signal-to-noise ratio is a problem which limits the usefulness of EM. Two-dimensional (2-D) arrays provide a means to overcoming this signal-to-noise ratio problem by allowing averaging of the structural EM data over many unit cells. However, structural information for large macromolecules is often limited by the problem of obtaining well-ordered crystals. Heterogeneity in the crystals may be due to a variety of factors including complexity of the structure (many, variably expressed subunits); deformability (because of weak inter-subunit interactions) and variable post-translational modifications of subunits [3]. This may lead to mosaic arrays with poor long-range order. In many cases, even poorly ordered arrays are unobtainable, and under these conditions structural data has to be derived from randomly oriented systems. In this situation, signal-to-noise problems have been overcome by averaging images of many particles with similar projections (relative to the electron beam) [4]. In order to carry this out, the images of the particles have to be first classified into groups displaying similar projections; and then within each group, the particles have to be translationally and rotationally aligned versus a reference particle selected from the group. The main drawback however, is that the success of the rotational and translational alignment depends on the signal-to-noise ratio of each individual image. Nevertheless, such methods have significantly enhanced the structural information obtained for many large macromolecular assemblies such as the ribosome [5], proteasome [6], nuclear pore complex [7] and chaperonins [8]. Here, for the first time, we show that the same methods are particularly effective when applied to partially ordered systems: i.e., in 2-D protein-lipid arrays which are ordered to such an extent that lattice refinement procedures are precluded. Due to the confinement of the lipid environment, thus fixing all the particles along the z-axis (i.e., they are aligned along the axis perpendicular to the membrane plane), they only exhibit rotational freedom within the x, y plane, and therefore the effectiveness of the rotational alignment procedures and its dependence on signal-to-noise ratio can be assessed. It would, however, be extremely difficult to assess the rotational alignment for solubilised protein in this way. This also enables one to use relatively fewer projections for SPA since the molecules are fixed in one-dimension [9] and, therefore, after alignment the molecules can represent the same view or a similar class of molecule and it is possible to use less than 100 molecules for the final average [5].

Photosystem II (PS II) is an example of a large (> 800 kDa), complex (> 20 subunits) membrane protein involved in photosynthesis [10] that forms 2-D arrays in its native thylakoid membrane. This has led to 3D structural data at 3 nm and recently 1.8 nm resolution [11,12]. We aimed to study the removal and rebinding of extrinsic subunits from these arrays in order to learn more about the subunit architecture of the complex. However, the method used to reversibly remove the subunits (0.5 M $CaCl_2$ washing) led to a significant deterioration in the quality of the semi-ordered protein-lipid arrays. Hence it was decided to investigate the possibility of using SPA methodology as described above to carry out the structural analysis and locate the positions of the extrinsic subunits.

The extrinsic subunits of PS II have been extensively studied biochemically, and it is known that they are located on the lumenal face of the thylakoid membrane. Three extrinsic polypeptides, OEE-33 (33 kDa), OEE-23 (23 kDa), and OEE-16 (16 kDa) play important roles in water oxidation and together form the oxygen-evolving complex (OEC) [13–15]. The 33 kDa protein appears to be required for stabilizing the higher oxidation states of manganese produced by photoreactions of PS II [16,17]. The 23- and 16-kDa proteins are also important for binding Ca^{2+} and Cl^{-} [18] and are thought to play regulatory or structural roles. These hydrophilic extrinsic proteins are loosely bound to the PS II membrane [19] and various workers have eluted them with chaotropic agents, (leaving the Mn still bound to the complex) [20] followed by subsequent rebinding in low ionic-strength buffer [21,22]. It was observed in these experiments that the dissociation of these proteins resulted in an increased requirement for chloride [23] and calcium ions [24] in order for maximal oxygen evolution to occur. Successful rebinding was variable in their experiments and therefore in this study we monitored the process by Coomassie staining of polypeptides separated by

SDS-PAGE and also by labelling the extrinsic subunits with a 55-atom gold cluster that allowed the visualisation of the subunits on SDS-PAGE.

There is a considerable debate concerning the oligomeric form of the PS II complex with evidence for both monomeric [11,12,25] and dimeric structures [26,27,40]. We now attempt to settle the controversy by calculation of the shape and assignment of the domain molecular architecture of the PS II complex using SPA and also by assessment of the rotational alignment of the PS II particles with respect to selected reference molecules.

2. Materials and methods

2.1. Materials

Spinach (*Spinacea oleracea*) was obtained from a local supermarket. The chlorophyll *b*-deficient *chlorina-f2* mutant of barley was kindly supplied by Dr David Simpson (Carlsberg Research Laboratories, Copenhagen) and grown in a glasshouse in vermiculite for 7 days with a 10 h photoperiod under natural lighting conditions. Triton X-100, uranyl acetate were supplied by BDH (Merck), Hunter Boulevard, Lutterworth, Leicestershire. DMBQ and the borane-dimethylamine complex (DMAB) were supplied by Aldrich, Gillingham, Dorset, UK. Aurothioglucose, potassium ferricyanide, Ponceau S solution, the silver enhancement kit and sodium thiosulfate were supplied by Sigma, Poole, UK. NANOGOLD reagent was purchased from Nanoprobes, Stony Brook, NY. The Bio-Rad Protein assay kit and molecular mass markers were supplied by Bio-Rad, Hemel Hempstead, Hertfordshire, UK. Copper 300 mesh/inch, ILFORD EM film and ILFORD Phenisol developer were supplied by Agar, Stansted, Essex, UK.

2.2. Photosystem II preparation

PS II was isolated from spinach as described by Ford and Evans [28] and was stored in 20 mM Mes, 5 mM $MgCl_2$, 15 mM NaCl, 20% (v/v) glycerol pH 6.3 (resuspension buffer) at −80°C. The barley *chlorina-f2* PS II membranes were prepared as described by Bassi et al. [29]. The membranes were stored in 20% (v/v) glycerol in 20 mM Mes (pH 6.3), 15 mM NaCl and 25 mM $MgCl_2$.

The oxygen evolution activities of the PS II membranes were measured using a Clark-type oxygen electrode (Rank, Bottisham, Cambridge, UK) at 20°C. The oxygen assay buffer consisted of 20 mM Mes (pH 6.5), 15 mM NaCl, 5 mM $MgCl_2$ and 20% (w/v) glycerol with 4 mM DMBQ and 1 mM potassium ferricyanide as electron acceptors. The oxygen electrode was illuminated by light from a 1000 W tungsten filament lamp with a flat 1 litre Roux bottle containing 1% w/v copper (II) sulfate as a heat filter.

2.3. Dissociation of extrinsic proteins

PS II membranes were treated with 0.5 M $CaCl_2$ in resuspension buffer at 0°C (20 min). All preparative procedures, thereafter, were conducted in the dark or subdued light. The membranes were collected by centrifugation ($10\,000 \times g$, 8 min, 4°C) and washed in low ionic-strength incubation buffer (70 mM sucrose, 30 mM sodium phosphate, pH 6.5 and 3 mM NaCl).

The supernatant containing the extrinsic proteins was diafiltrated in 20 mM Hepes (pH 7.5) with an Amicon Centriprep-10 (cut off 10 kDa) ultraconcentrator (Amicon, Gloucestershire, UK). For labelling of extrinsic proteins, the NANOGOLD was dissolved in 0.2 ml of deionized water (the reagent was lyophilized from 20 mM Hepes-NaOH at pH 7.5) and the activated NANOGOLD solution immediately added to the protein and incubated for 1 h at room temperature. Sufficient reagent was supplied to label 1.2 nmol of amine sites and based on the number of moles lysine per mole of protein [16], the optimal amount of extrinsic proteins to add to the NANOGOLD was calculated. This was also confirmed by titrating the extrinsic proteins with a range of NANOGOLD concentrations (data not shown). The labelled proteins were concentrated by ultrafiltration at 4°C and desalted into incubation buffer.

2.4. Rebinding of extrinsic proteins

Labelled protein and calcium chloride washed membranes were incubated at increasing protein to Chl ratios in low ionic-strength incubation buffer for

1 h in the dark at 4°C, up to a protein to Chl ratio of 2:1 (w/w) [22,30]. The resulting changes in oxygen evolution activity were recorded using a Clark-type oxygen electrode, as described above. Membranes were then applied to a continuous sucrose gradient (1–2 M) to remove any non-specifically associated NANOGOLD and concentrated by centrifugation at $10\,000 \times g$ for 10 min (4°C), followed by further washing to remove any randomly associated protein.

2.5. SDS-polyacrylamide gel electrophoresis

Protein concentrations were measured using a Bio-Rad protein assay kit [31] with lysozyme as a standard. Samples were run on an SDS-PAGE gel (mini-protean II electrophoresis cell supplied by Bio-Rad, Hemel Hempstead, Hertfordshire, UK) as described by Laemmli [32]. Samples were mixed 1:1 with buffer containing 125 mM Tris-HCl (pH 6.7), 6% (w/v) SDS, 40% (w/v) glycerol, 0.02% (w/v) bromophenol blue and 10 mM dithiothreitol and run at 200 V for 45 min on a 15% acrylamide slab gel. Proteins were stained in 0.1% (w/v) Coomassie blue G-250 in 40% (v/v) methanol and 10% (v/v) acetic acid for 2 h followed by destaining in 40% (v/v) methanol and 10% (v/v) acetic acid.

For electroblotting, SDS-PAGE was undertaken as described above except borane-dimethylamine complex (DMAB, 10 mM) replaced dithiothreitol in the sample buffer since thiol reagents destroy the gold cluster rapidly [33]. Electroblotting was performed as described by Hartvig and Capaldi [34] using a Biometra FastBlot apparatus (Biometra, Göttingen, Germany). The protein was transferred onto nitrocellulose by 'semi-dry' blotting between carbon plate electrodes transferring at 100 mA for 1.5 h, in transfer buffer containing 0.1% (w/v) SDS and 20% (v/v) methanol. The nitrocellulose was stained with 0.02% (w/v) Ponceau S solution to detect protein. This was then rinsed with deionized water and a silver enhancement kit was used for colour development of the NANOGOLD-labelled protein lanes, followed by fixing the gel in 2.5% (w/v) sodium thiosulfate. Gels were photographed and then printed. The prints were analysed by densitometry using a PC-based image analysis system to provide a quantitative assessment of rebinding (indicated by NANOGOLD-labelled extrinsic proteins bound to appropriate PS II membrane protein samples) shown by the silver-enhanced gels.

2.6. Electron microscopy

Membranes with a chlorophyll concentration of 100 μg/ml were adsorbed to collodion-carbon coated, copper 300 mesh/inch grids, and freshly glow-discharged for 1 min under reduced atmospheric pressure. The grids were washed briefly and negatively stained with 2% (w/v) aqueous uranyl acetate or 2.5% (w/v) aurothioglucose and dried in air at room temperature [11]. Images were recorded with a Hitachi H-600 electron microscope at 100 keV at a calibrated magnification of 37 260 × and 18 630 ×, respectively. Minimal-dose methods were employed and electron micrographs were recorded on ILFORD EM film and developed in ILFORD Phenisol developer (diluted 1:4) for 4 min. Selected images were digitized in 25 micron increments with a Joyce-Loebl rotating drum microdensitometer.

2.7. Image processing

Single-particle averaging was undertaken with the SPIDER software package on micro-VAX and INDIGO-Silicon Graphics workstations [35,36]. The images were initially band-pass filtered [37] to supress noise. Particles (approx. 150 for each type of treatment [26]) were interactively selected using the program WEB, padded to 64×64 pixels and the densities normalised [38]. Padded images were masked with a circular mask and a Gaussian fall-off filter applied with a half-width of 1.0 pixel [4]. Particles were rotationally aligned by an autocorrelation function-based method [37] and translationally aligned by cross-correlation using a reference particle [39]. Initially, the particles were iteratively aligned with respect to a reference particle and the best aligned particles were used to calculate a new reference which was then used to align the remainder of the particles [37]. An average image was calculated by summing the aligned particles. For the calculation of the projection maps with a $p2$ plane group or as applicable for SPA, twofold rotational symmetrisation [26], the appropriate average was centred by establishing its centre of gravity and shifting the

molecule accordingly. It was then rotated 180 degrees and summed with its non-rotated counterpart [40].

The cross-resolution (reproducible resolution) was determined from two subaverages by phase residual analysis [4]. Subaverages were generated using different subsets of particles and the proximity between the two Fourier transforms compared in Fourier space. The differential phase residual was computed by summation over rings in the Fourier plane and plotted as a function of ring radius. The 45 degree limit (half-random residual) was determined and the resolution was extrapolated.

3. Results

Fig. 1 shows a montage of electron micrographs of negatively-stained PS II molecules in grana membranes showing densely packed stain-excluding particles with regions of 2-D ordered arrays. Note that the arrays are irregular in form with many deformations of the lattice and poor long-range order. Fourier transformation of many of such images gave at best only one or two orders, representing very low resolution information. Estimates for unit cell dimensions of such arrays are detailed in the figure legends. Note that the contrast for aurothioglucose stained membranes (Fig. 1b) is considerably weaker than for the uranyl acetate stained specimen, giving a lower signal-to-noise ratio for the aurothioglucose-stained membranes. This provided a useful comparative test for the effectiveness of SPA methodology.

Single particle alignment was carried out on particles selected directly from the 2-D arrays and the success of the rotational alignment procedure was assessed. The success of the alignment was adjudged if the molecules were rotationally aligned with respect to their crystallographic a and b axis (which could be readily assessed by this method as the molecules were part of 2-D arrays) and whether they were aligned 0 or 180 degrees (± 10 degrees) with respect to a reference molecule. No differentiation between 0 or 180 degree cases was initially considered because these two orientations would be equivalent if the plane group symmetry was $p2$ as discussed earlier. For a $p2$ space group [26,40], one would expect the correctly orientated particles to be split roughly 1:1 between 0 and 180 degree orientations. However if the space group were $p1$, as suggested by others [11,12], then one would expect an large uneven split between the 0 and 180 degree

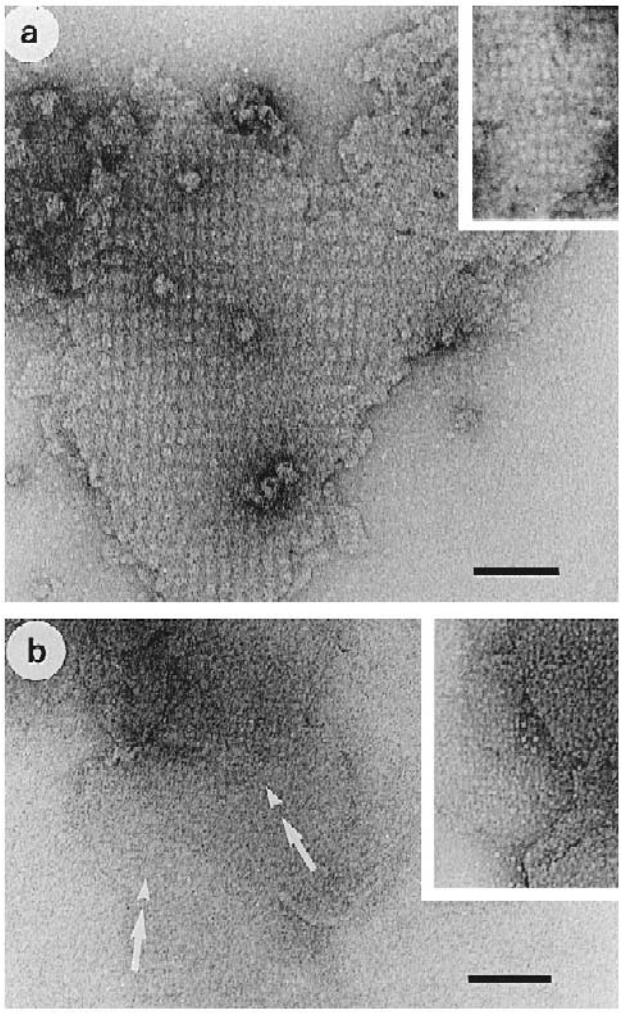

Fig. 1. Electron micrographs of negatively-stained membranes containing 2-D arrays of PSII. (a) Control, untreated barley (*chlorina-f2)* PSII membranes stained with 2% (w/v) uranyl acetate on carbon-collodion copper EM grids. Protein appears as white surrounded by dark stain. Note that even in control membranes some long-range disorder in the crystal exists. Unit cell dimensions were 15×21 nm with γ approx. $= 90°$. The inset shows similarly stained membranes after rebinding of extrinsic proteins to $CaCl_2$ washed barley membranes. (b) Calcium chloride-washed spinach PS II membranes stained with 2.5% (w/v) aurothioglucose, with the arrows pointing to areas containing 2-D arrays. Unit cell dimensions were estimated as 15.5×20 nm with γ approx. $= 90°$. Note the low contrast and signal to-noise ratio with this stain. The inset shows spinach PS II membranes under the same conditions except after rebinding of extrinsic subunits. Scale bars are 100 and 200 nm for a and b, respectively.

aligned particles, especially where high signal-to-noise ratio images were available, and the ratio of 0 to 180 degree orientations would deviate markedly from 1:1. Thus, as a second exercise, we categorized the particles into 0 and 180 degree aligned categories, i.e., particles which showed maximum correlation with the reference by a rotation angle of 0 or 180 degrees. We were not concerned, at this stage, whether the 0 or the 180 degree class had a larger number of molecules since it was unclear whether the reference should be at 0 or 180 degrees. Table 1 summarizes the results obtained after rotational alignment applied to the differently treated 2-D arrays of PS II. For all treatments the split between 0 and 180

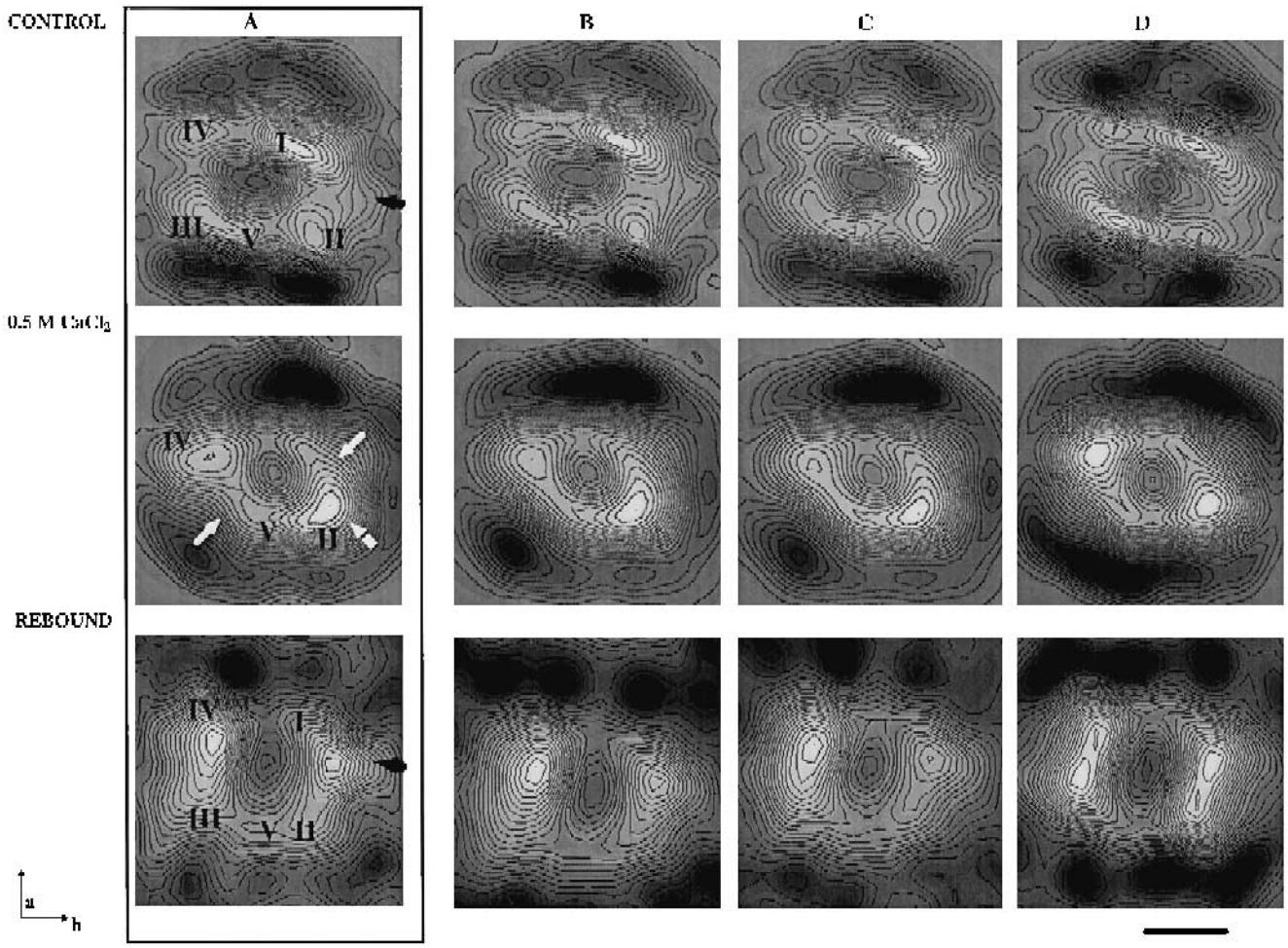

Fig. 2. Single-particle alignment showing averaged projection maps of barley (*chlorina-f2*) PS II membranes stained with uranyl acetate. Contours and shading were used to represent density variation due to stain (dark areas) and protein (light areas). Control, untreated barley *chlorina-f2* membranes with the five major domains (I–V) and labelled as in Ford et al. [12] is shown. Calcium chloride washed membranes (the positions of the missing domains are shown by white arrows with a broken arrow shown for the loss of domain II as discussed in the text) and the extrinsic proteins rebound is also shown. The thick black arrow indicates a protrusion on the complex discussed in the results section. For orientation purposes, the relative directions of the a and b axes of the 2-D arrays are shown. For the control, the effects of misalignment are shown in columns A, B and C where column A shows the average using particles in the major alignment category (0 or 180 degree), B shows the average with particles rotated 180 degrees with respect to column A included in the average; and column C shows the average of all particles irrespective of the rotational alignment. Column D shows the twofold rotational symmetrised image as discussed in the methods and materials section. The approximate resolutions of the images of uranyl acetate stained PS II were 35Å using the phase residual consistency test. This resolution value appeared to correspond to the sizes of general features observed in the images. Scale bar = 8 nm. See text for further details.

Table 1
Effectiveness of rotational alignment by SPA subroutines for membrane-bound PS II complexes in 2-D arrays after various treatments and different staining conditions

	Control U	Washed U	Rebound U	Washed Au	Rebound Au
Aligned:					
0 degree	65	22	40	21	13
180 degree	10	44	30	5	6
Total aligned	75	66	70	26	19
Total misaligned	25	34	30	74	81

Results are expressed as percentages.
U, uranyl acetate stained; Au, aurothioglucose stained.
Washed – extrinsic subunits removed by 0.5 M $CaCl_2$ wash.
Rebound – extrinsic subunits rebound to the membranes in low ionic strength buffer (70 mM sucrose, 30 mM sodium phosphate, pH 6.5 and 3 mM NaCl) after removal of salt.

degree orientations is uneven with a maximum differentiation occurring for uranyl acetate stained PS II where the ratio of the split was as high as 86:14. These data therefore independently support a space group assignment for PS II 2-D arrays of *p*1 rather than *p*2.

The majority of particles (66–75%) were successfully aligned for the uranyl acetate stained specimen, but the success rate dropped significantly for the aurothioglucose-stained specimens (26%). The signal-to-noise ratio in the images obtained for uranyl acetate stained specimen was estimated to be about 2.2:1, whilst for the aurothioglucose-stained situation the ratio was estimated as about 1.3:1. Thus lower signal-to-noise leads to lower success at correct rotational orientation, as expected.

Following on from this, the effect of misalignment in SPA studies was investigated by calculating averages of projection maps for the PS II complexes under four different conditions (Figs. 2 and 3, A–D). For one category (column C), all particles were included irrespective of their orientations. In another category (column B), aligned particles with both 0 and 180 degree rotations were selected and averaged. In the last category (column A) only particles in the major category (0 or 180 degrees) were used. Finally, a 2-fold rotational symmetrisation was applied to the molecules denoted in column A (column D). Figs. 2 and 3 summarize the results and shows the effect of

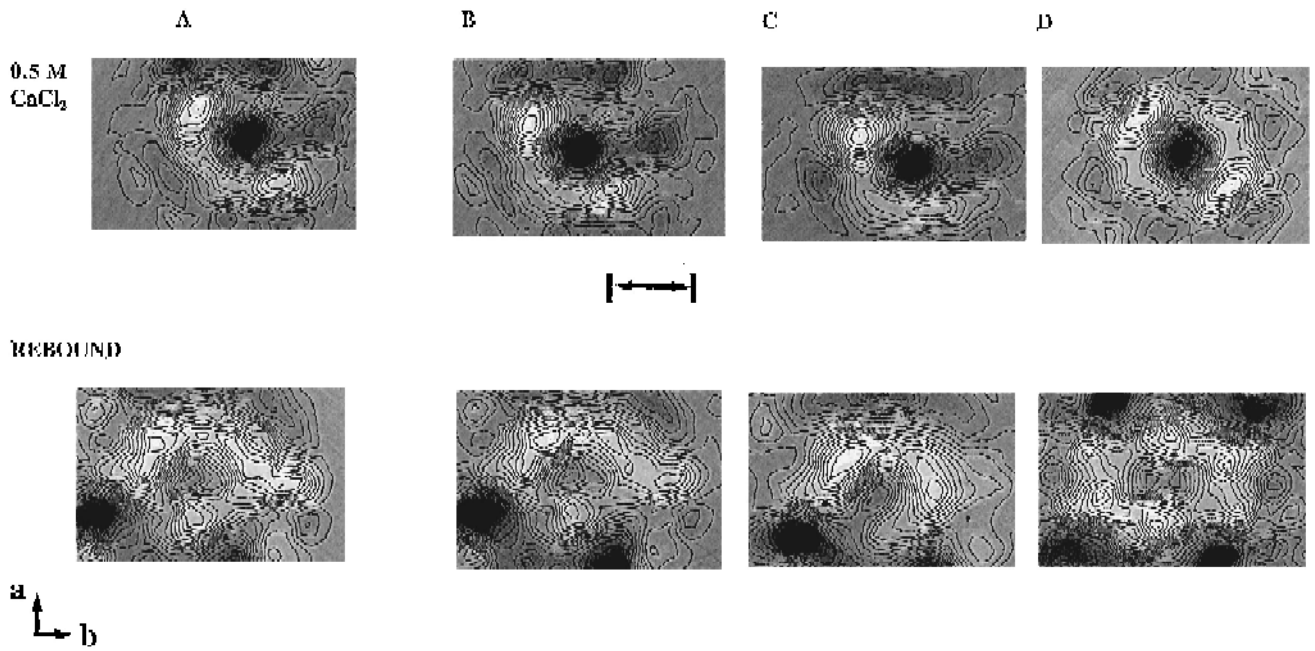

Fig. 3. Single-particle alignment showing averaged projection maps of PS II stained with aurothioglucose. Calcium chloride washed spinach PS II membranes and after rebinding of extrinsic proteins is shown. The relative orientation of the a and b axes are shown. The effects of misalignment on the averaged projection maps are displayed in columns B and C with the twofold rotational symmetrised space group image in column D as described in Fig. 2. Scale bar = 8 nm.

the misalignment on the final average. In Fig. 2 incorrect alignment causes the domains to be less defined and hence appears to have a higher symmetry. This effect is most prominently illustrated in Fig. 2, rebound, where domains I, II, III and IV in the correctly aligned average merge to give a bilobed structure (columns B and C) while incorrect alignment also leads to a more rounded structure with the longer axes compressed and the shorter axes extended. This effect might be expected when averaging over particles aligned approximately perpendicular to each other (in the membrane plane). This effect is also observed for aurothioglucose-stained specimens (Fig. 3) where the signal-to-noise ratio is poor. These results have general significance for understanding the problems associated with SPA of non-aligned specimens, where the rotational alignment procedure cannot normally be verified (see later).

After twofold rotational symmetrisation (Figs. 2 and 3, column D), the molecules appear to be at a poorer resolution indicated by a 'smearing' of the domains which is especially evident for the asymmetric uranyl-acetate stained calcium chloride washed structure (with an apparent decrease in its volume). Furthermore, the 0.5 M calcium chloride washed uranyl-acetate stained PS II complex becomes similar to the control and rebound structures after symmetrisation. Also, the loss of the 'nose' for the control and rebound structures, which we have shown to be a consistent and important feature across different strains of PS II [Flint et al. submitted, 1996], questions the allocation of a $p2$ space group and not a $p1$ space group for PS II.

Studies of PS II 2-D arrays after $CaCl_2$ washing to remove extrinsic subunits were hampered by reduction in the quality of the 2-D arrays after the washing procedure. The reasons for this may be due to a chaotropic effect of the salt leading to a noticeable weakening of protein–protein interactions within the array. Therefore SPA was used throughout this study for consistency even when ordered arrays were encountered e.g. with the control (untreated) PS II membranes. Fig. 2 in addition, therefore, shows the affect of treatment of native or control PS II with calcium chloride to remove the extrinsic proteins which are subsequently rebound. For control PS II (Fig. 2A) the averaged projection map displayed a central stain cavity with a diameter of approximately

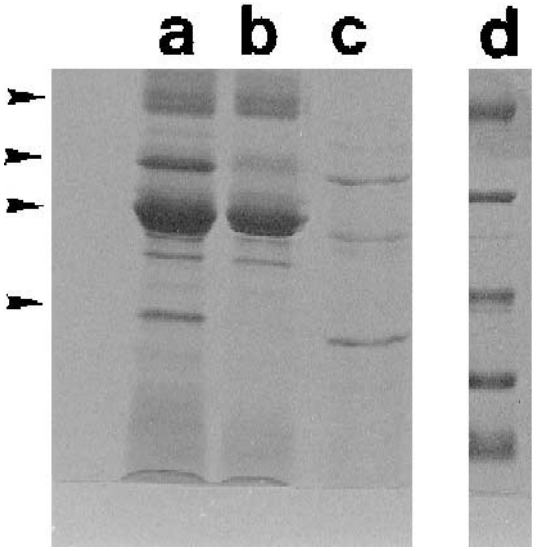

Fig. 4. Representative SDS-PAGE showing native and calcium chloride washed spinach PS II membranes and the supernatant containing the extrinsic proteins. Lane a, intact PS II and lane b shows PS II membranes treated with 0.5 M $CaCl_2$ for 20 min on ice in the dark and collected by centrifugation ($10\,000\times g$, 3 min, 4°C) and resuspended in incubation buffer. Approx. 8 μg of chlorophyll was loaded in each track. Lane c shows the supernatant after centrifugation containing the extrinsic proteins, i.e., 33, 23 and 16 kDa proteins. These have migrated slightly differently relative to the PS II due to the presence of some residual salt. Lane d shows the molecular-mass markers of 45, 31, 21, 14.5 and 6.5 kDa from top to bottom. Arrows point (from top to bottom) to CP47/43 (and the band above possibly aggregated protein which is common in PS II preparations), the 33 kDa protein (and at 34 kDa the D1/D2 proteins), the LHCII proteins and the 16 kDa extrinsic protein, respectively. For lane b, note the marked loss of the 33, 23 (narrowing of LHCII area) and 16 kDa protein with their concomitant elution into the supernatant (lane c).

3.5 nm surrounded by five domains (I–V) which have been described in previous reports [11,12,41,42]. This structure is also confirmed in Fig. 5a which was calculated from well ordered 2-D crystals by Fourier reconstruction methods. This projection represents the lumenal side of the complex where the stain tends to accumulate [11,12]. Interestingly, the projection displays a small 'nose-like' protrusion at one end of the complex (arrowhead) whilst a more rounded surface is revealed at the opposite end. These asymmetric features have also been previously observed [11,12] in native PS II but are largely absent after Tris-treatment [12] and are positive indications for

the assignment of the *p*1 space group. Fig. 2 also shows the PS II projection after calcium chloride washing. The structure is dramatically altered with the loss of domains I and III (arrows), an attenuation of domain II (broken arrow) whilst domain IV and V remain intact.

In order to properly assess the changes of the untreated/calcium chloride treated PS II, the two averaged images were rotationally and translationally aligned and a difference map was calculated. Peaks in the difference map suggested protein removal occurred at three separate locations which corresponded to domains I to III (Fig. 6). The maxima for domain II was not as large compared with domains I and III which correlates with visual inspection of the map

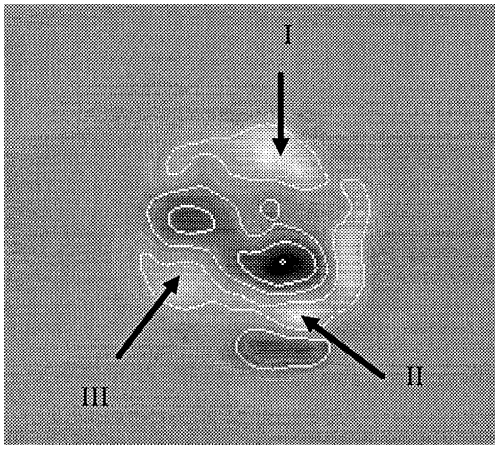

Fig. 6. Difference map of untreated minus calcium-chloride-treated chlorina f2 photosystem II. Peaks occurred at three separate locations corresponding to domains I to III.

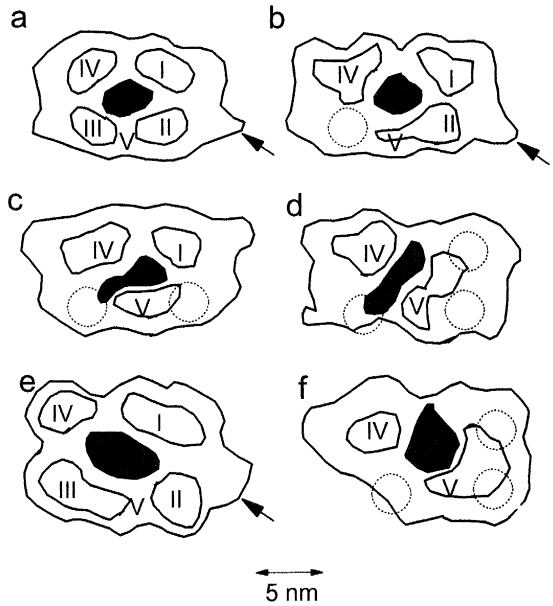

Fig. 5. PS II projection maps after various salt treatments. Molecular outline and positions of the strongest peaks are represented. Roman numerals are used for identification of domains using previous nomenclature [11]. Dotted circles show original positions of domains I, II and III where they are removed. Shaded areas show positions of a central stain filled cavity or channel. Arrows point to features previously described as the 'nose' on the complex. Contours were drawn from projection maps of (a) native PS II spinach 2-D arrays [11] (b) 0.25 M NaCl wash spinach crystals where the 16 kDa protein has been lost [43], (c) 1 M NaCl washed PS II crystals where the 16 and 23 kDa proteins have both been lost [43], (d) Tris washed PS II crystals where all extrinsic subunits are removed [41] (e) native barley PS II as in Fig. 2 obtained by SPA (f) 0.5 M CaCl2 washed PS II as in Fig. 2 by SPA.

shown in Fig. 2 and is thus represented as a broken arrow in this figure. This is likely to be due to domain V, which is only clearly revealed after removal of domains I, II and III, lies partially under domain II in the native structure [12] thus making domain II removal difficult to visualize in the map of the negatively-stained complex.

The action of $CaCl_2$ is similar to that of 1 M Tris which also removes the 3 extrinsic polypeptides. The projection map that we determined by SPA does indeed show similarities to Tris-treated 2-D arrays [41] with the presence of 2 major domains separated by a channel running across the face of the complex (Fig. 5d); this also shows that well-ordered crystals can give similar results to SPA. Fig. 2 also shows the projection after the extrinsic proteins have been rebound to the complex, with a large restoration of the original shape of the molecule. The projection map appears slightly different to that described previously [49] due to it being at higher resolution by including more particles and by applying a slightly tighter mask. The restoration of the original shape is significant yet not complete. This observation is likely to correlate with an incomplete rebinding of extrinsic subunits to the complex [21,22] although an increase in oxygen-evolution activity was observed suggesting the extrinsic proteins had re-bound. We estimated the degree of rebinding by using Coomassie stained gels and also electroblotting and silver enhancement of gold-labelled subunits to visualize the rebinding pro-

Table 2
Abundance, extent of removal and rebinding of extrinsic subunits of PS II to PS II-enriched membranes as detected by Coomassie staining and silver-enhancement staining of polypeptides separated by SDS-PAGE

	Control [a] (Coomassie)	Washed [a] (Coomassie)	Rebound [a] (Coomassie)	Rebound (+Nanogold) [b]	Supernatant from wash (Coomassie) [b]
33 kDa	12.3	0	5.4	9.7	12.5
23 kDa	8.2	0	4.6	4.3	8.5
16 kDa	5.9	0	4.7	12.6	3.2
	%	%	%	AU	AU

[a] Relative magnitudes of the polypeptide band relative to the major LHCP band.
[b] Values taken directly from the densitometer readings (AU – arbitrary units).
(+Nanogold) – silver-enhanced bands were measured on the electroblot. These appeared at positions corresponding to the subunit molecular mass plus 15 kDa (the mass of the Nanogold label). The 16 kDa protein had rebound to the greatest extent (12.6) which reflected the results from Coomassie staining showing 80% rebinding.

cess. The gel in Fig. 4 confirmed that the native PS II complex (track a) had lost the three extrinsic proteins after washing with calcium chloride (track b) which were the major proteins found in the supernatant (track c). Another gel was then run with a track including rebinding of the extrinsic proteins to PS II. After visual inspection of the gel it was clear that it was necessary to scan the rebound track in order to achieve a greater quantitative estimation of rebinding. Quantification of the intensities of the bands by densitometry led to estimates for the relative extent of rebinding for the 3 subunits, as reported in Table 2. The results from Coomassie staining of the gels show that partial rebinding is the norm for all 3 subunits, with the strongest rebinding observed for the 16 kDa subunit (about 80% of the native amount) and weakest for the 33 kDa subunit (about 45%). These results are largely confirmed by the NANOGOLD labelling results, where the 16 kDa subunit is again most strongly rebound (with this method, it is the 23 kDa subunit which is the least strongly bound). The data from these studies can be used to help the interpretation of the projection maps of PS II. We suggest that there are 3 separate locations for the extrinsic subunits on the face of the complex corresponding to domains I, III and (partially II) in the native complex. Domain II appears to be the least recovered in Fig. 2, rebound. Thus from the projection maps, the behaviour of domains I and III appear to correspond to the rebinding of the 16 and 33 kDa subunits, whilst domain II appears to be the more likely location of the 23 kDa subunit. Similar conclusions have been arrived at recently using sequential removal of the subunits [43].

In Fig. 3, the average projection maps obtained by SPA for PS II stained with aurothioglucose are shown. Because of the weaker contrast as well as the fact that fewer particles align correctly, the projections contain considerably more variation due to noise and there is little consistency in the images produced. The effects of translational misalignment, which is likely to significantly affect these low signal-to-noise ratio images, would cause the average structure to blur leading to a potential loss of resolution. This is seen in the figure, with the rotationally aligned particles (column A) having little domain substructure. Rotational misalignment induces an apparent symmetry (column B) with a more spherical delineation (column C). The only consistent difference between $CaCl_2$-washed PS II and PS II with extrinsic subunits rebound was that the large central staining area becomes smaller and better defined after rebinding. However, it is clear that SPA studies with aurothioglucose should be treated with extreme caution.

4. Discussion

In this report we have shown that SPA can be effectively applied to the analysis of small and/or poorly ordered 2-D arrays, thus extending the range of possibilities for structural analysis by electron microscopy. It is anticipated that many large and highly complex macromolecules could form only

weakly ordered arrays (if at all), and therefore this methodology may become of increasing importance for low to medium (5 to 1 nm) resolution structural studies. In addition, with the rapid expansion of the number of (3D) crystallization trials taking place on both soluble and membrane protein complexes, the methods we describe could be important in the structural analysis of a significant category of proteins that only form weakly ordered microcrystals which are unsuitable for X-ray crystallography. Such 3D crystals can be examined by EM after embedding and sectioning [44].

SPA is a valuable technique for the analysis of randomly ordered protein complexes, and in some cases is the only practical way of obtaining structural data. However, with low signal-to-noise data such as in cryo-electron microscopy of unstained preparations or aurothioglucose-stained specimens (as in this report), the technique must be applied with some caution. The data that we have presented suggests that with low signal-to-noise ratio images of particles, the success rate for correct rotational alignment is low. The effects that this has on the final averaged structure is to induce a blurring with a possible tendency towards symmetrisation. Thus low signal-to-noise projection maps that are produced by SPA must be viewed sceptically where information on oligomeric nature of the protein complex is desired. A possible solution to this problem is to align low signal-to-noise ratio particles against a much higher signal-to-noise reference particle (e.g. one obtained from uranyl acetate staining). This has recently proved effective for analysis of cryo-electron microscopy images of unstained ribosomes [45].

We have also found that analysis of SPA rotational alignment results can help considerably in the independent assignment of space group for 2-D arrays, and the rotational alignment results that we describe for PS II in Table 1 provide further evidence against a dimeric model of native PS II due to the large split between 0 and 180 degree aligned molecules. The projection maps also calculated by SPA (Fig. 2) show a clear asymmetry as expected for a monomeric complex and Fig. 2 (control) also correlates closely with data from ice-embedded specimens at 3.5 nm resolution [46] thus negating the arguments of negative-stain artifacts.

The location of the extrinsic subunits of PS II have been studied in this report and in others. Simpson [47] showed by freeze-fracture electron microscopy, fracture faces displaying numerous tetrameric particles on the endoplasmic surface of thylakoids and concluded that the extrinsic polypeptides of the oxygen evolving complex were the major components of the these particles. Seibert et al. [48] showed that the tetrameric particles disappear upon removal of the extrinsic proteins. The dimeric structure that is revealed can revert to a tetrameric form on rebinding of the extrinsic proteins. These findings largely concur with the changes shown in Figs. 2 and 3 and the tetrameric particles were also of a similar size. However, this is the first time the rebinding has been studied by EM and image analysis. We show that rebinding leads to a large restoration of the original shape of the PS II complex with a partial return of the domains (I, II and III) that have been attributed to the lumenal extrinsic proteins [43] and that the lumenal portions of the transmembrane proteins CP47 and CP43 (domains IV and V) [12] are unchanged. These studies do not rule out the possibility of non-specific binding of any of the extrinsic subunits, but since the image analysis averages over many complexes, it is likely that non-specific binding at multiple sites would be averaged out and hence not observed in the final projection maps (Figs. 2 and 3). In general, though, the extent to which domains I, II and III recover in the projection maps, does appear to correlate with the extent of rebinding, as detailed in Table 2.

The various structural studies [11,12,43,49] describing the location of the components on the lumenal side of PS II are summarized schematically in Fig. 5. Native PS II in 2-D crystals of spinach (a) and barley (e) correspond closely, as expected, confirming the efficacy of the crystallographic (a) and SPA (e) image analysis methods. Four main domains (I–IV) are assigned, whilst domain V lies partially buried underneath domains II and III and is only fully revealed after removal of the 23 and 16 kDa subunits [12] (Fig. 5, d and f). Removal of the 16 kDa protein by 0.25 M NaCl treatment (b) results in a structure that is little changed, except for a reduction in domain III. A harsher 1 M NaCl treatment (c) results in the removal of the 16 and 23 kDa proteins and is manifested in a reduction in domains II and III in the structure. Removal of all the extrinsic proteins by 1 M Tris treatment (d) or 0.5 M $CaCl_2$ treatment (f)

leads to the loss of domains I, II and III, whilst domain IV is relatively unchanged and domain V becomes more readily apparent. Note that in both projection maps (d) and (f) domain V extends upwards and across from a position midway between the binding sites of domains II and III to a position close to the binding site of domain I. In summary, therefore, the assignment of domains I, II and III to the 33, 23 and 16 kDa subunits, respectively [43] appears to be consistent with all the data presented here.

Fig. 5 also aids in the discussion of the oligomeric form of the complex. From the overall distribution of the OEE subunits within the complex or especially after removal of the 23 and 16 kDa (c) while leaving the 33 kDa protein or after the loss of only the 16 kDa protein (b) the complex has a strong asymmetric character. Such an asymmetry would be unlikely if the PS II was a dimer.

Due to there being $>95\%$ homology between barley and spinach PS II subunits no significant differences would be expected at this resolution and this enabled us to compare the data in Fig. 2 with Fig. 5. Moreover, the strong similarities between Fig. 5a spinach (control) [11,12] and Fig. 5e *chlorina-f2* (control) show clearly that the systems are directly comparable.

There appears to be some confusion in the literature concerning the oligomeric form of PS II. The effect of oligomerization after detergent solubilization [42] has been proposed to explain many of the inconsistencies in reports describing monomeric, dimeric or tetrameric structures [26,50], whilst other reports (for purified PS II in 2 D crystals [40,51,52]) are possibly explained by the constraints of packing within the 2-D unit cell, i.e., $p2$ or $p22_12_1$ packing in a crystal does not necessarily infer that this structural interaction is present in the native membrane. It should be noted, however, in the present study, the PS II complexes remained membrane bound. If the data for non-solubilised PS II in its native membrane are considered, then we find that low resolution studies [13,53] favour a dimeric structure, whilst studies at higher resolution [12,46] are more consistent with a monomeric behaviour. Because the complex is expected to have a pseudosymmetry (it is built around a heterodimeric reaction core) it is not surprising that the low resolution studies can readily be interpreted as showing dimeric structure. Where the PS II mass has been measured directly by STEM [25] then a monomeric complex was determined and the projection maps appeared very similar to those in Figs. 2 and 3. Interestingly, these data strongly concurs with earlier theoretical calculations of PS II mass and hence size using known subunit and pigment stoichiometries [11,12]

Similarly, confusion has arisen over the size of the observed complexes because of variable oligomerization of PS II complexes that have lost some of their original subunits. For example, the core dimer described by Boekema et al. [26,50] is a detergent-extracted complex containing subunits CP47, CP43, D1, D2 and cyt b559, but completely lacks the peripheral light harvesting antennae subunits. Its overall dimensions (17×10 nm) reflect the compact size of the PS II core. Only two large stain excluding domains were observed for the core monomer suggesting that CP47 and CP43 subunits dominate projections of the core complex. In contrast, a supercore dimer described by Boekema et al. [26] contains core subunits (CP47, CP43, D1, D2, cyt *b*-559) but also contains some peripheral antennae proteins (CP29, CP26, $3 \times$ LHCII) although these are considerably depleted compared to the native PS II structure. This dimer is much larger with dimensions 30×18 nm. If we compare the dimensions of these dimeric structures with native PS II (20×16 nm) we can readily see that a dimeric form (for the native PS II) is ruled out. Clearly the supercore dimer (30×18 nm) which is already depleted in some LHCII subunits as well as lipid is too large to fit into the native unit cell (20×16 nm). A dimeric core complex (17×10 nm) is just small enough to fit into the unit cell, but this PS II core complex contains no peripheral light harvesting proteins that contribute at least 50% of the total mass of the native complex. Thus, it would be unacceptable to try to predict the oligomeric form of the native complex based on a highly depleted core complex. We suggest that the monomeric core complex (10×8 nm) is probably of a similar size to the portion of the native complex delineated by domains IV and V (Fig. 5). If one imagines this area of the native complex being extracted and separated from the remainder of the PS II subunits, then by allowing it to dimerize a complex of about 17×10 nm could possibly be created. This argument may also apply to

the dimeric core complex reported by Lyon et al. [40] of 16.1 by 11.5 nm where extrinsic proteins and peripheral antennae proteins are missing.

It should be noted that it is misleading to estimate the size of the native complex (Figs. 2 and 3) by using contour lines enclosing the centre of the complex. Such measurements depend on the extent of negative-stain penetration, i.e., how far the complex protrudes from the hydrophobic membrane. We have recently shown from 3-D studies that the core-complex proteins protrude into the stain whereas the LHCII proteins are mainly buried within the membrane and are poorly stained [11,12]. For negatively stained material, therefore, the unit cell dimensions provide a more accurate representation of the size of the complex since it marks the extent of molecule to molecule lattice contacts.

The most important observation in this report was the removal of PS II extrinsic subunits and their subsequent rebinding and this has confirmed similar studies carried out by us on Tris-washed PS II 2-D crystals (where crystal order is maintained after the washing process) [12]. The resolution (3.5 nm) was suitable for observing changes to the features of the molecule as the extrinsic proteins were washed and then re-bound. It is presently thought that the three extrinsic subunits occupy separate locations on the lumenal surface of the complex and collectively surround a lumenal cavity that may be of significance for the mechanism of water oxidation [12]. Although the SPA studies presented here are at lower resolution, and are projection maps rather than 3D maps, the structural information derived from the SPA data can be strongly correlated with the 3D studies. In addition, since we have shown a reversible rebinding of the subunits and a concomitant return to the original structure, the possibility that the earlier Tris-treatment studies were complicated by gross conformational changes in PS II induced by Tris can be ruled out.

Acknowledgements

We would like to thank Dr Joachim Frank (NY State DoH), for useful discussions; Mr John Hutton and Mr Chris Gilkrist (EM Unit, Manchester Medical School), Mr Jim Mallet (Department of Chemical Engineering, UMIST) and Mr Paul McPhie (Department of Biochemistry and Molecular Biology, University of Leeds) for their technical assistance with the electron microscopy; Mr Don Akrigg (Department of Biochemistry and Molecular Biology, University of Leeds), Dr Tony Arnold and Mr Steve Larkin (Computer Graphics Unit, University of Manchester) for their computational assistance. We would also like to thank Dr Jaleel Miyan (Department of Biochemistry and Applied Molecular Biology, UMIST) for his invaluable discussions. We acknowledge the financial support of the BBSRC and The Leeds Centre For Molecular Recognition in Biological Sciences.

References

[1] Henderson, R. (1995) FASEB J. 9, A1256.
[2] Kuhlbrandt, W. and Gennis, R.B. (1994) Curr. Opin. Struct. Biol. 4, 517–518.
[3] Allen, J.F. (1992) Biochim. Biophys. Acta 1098, 275–335.
[4] Frank, J., Verschoor, A. and Boublik, M. (1981) Science 214, 1353–1355.
[5] Frank, J., Radermacher, M., Wagenknecht, T. and Verschoor, A. (1988) Methods Enzymol. 64, 3–35.
[6] Ikai, A., Nishigai, M., Tanaka, K., Ichihara, A. (1991) FEBS Lett. 292, 21–24.
[7] Reichelt, R., Holzenburg, A., Buhle, E.L., Jarnik, M., Engel, A. and Aebi, U. (1990) J. Cell. Biol. 110, 883–894.
[8] Chen, S., Roseman, A.M., Hunter, A.S., Wood, SP., Burston, S.G., Randson, N.A., Clarke, A.R. and Saibil, H.R. (1994) Nature 371 (6494), 261–264.
[9] Holzenburg, A. (1995) in Ion-Channels—A Practical Approach, Electron Microscopical Analysis of Ion-Channels (Ashley, R., ed.), pp. 269–290, IRL Press, Oxford.
[10] Vermaas, W. (1993), Ann. Rev. Plant. Physiol. Plant. Mol. Biol. 44, 457–81.
[11] Holzenburg, A., Bewley, M.C., Wilson, F.H., Nicholson, W.V. and Ford, R.C. (1993) Nature 363, 470–472.
[12] Ford, R.C., Rosenberg, M.F., Shepherd, F.H., McPhie, P. and Holzenburg, A. (1995) Micron, 26, 133–140.
[13] Santini, C, Tidu, U, Tognon, G, Magaldi, A.G. and Bassi, R (1994) Eur. J. Biochem. 221, 307–315.
[14] Ghanotakis, D.F. and Yocum, C.F. (1990) Annu. Rev. Plant. Physiol. Plant. Mol. Biol. 4, 255–276.
[15] Hansson, O. and Wydrzynski, T. (1990) Photosynth. Res. 23, 131–162.
[16] Yamamoto, Y., Nakayama, S., Cohn, C.L. and Krogmann, D.W. (1987) Arch. Biochem. Biophys. 255, 156–161.
[17] Kyle, D.J. (1985) Photochem. Photo. Biol. 41, 107–116.
[18] Ghanotakis, D.F., and Yocum, C.F. (1985) Photosynth. Res. 7, 97–114.

[19] Yamamoto, Y, Shinkai, H, Isogai, Y, Matsuura, K. and Nishimura, M. (1984) FEBS Lett. 175, 429–432.
[20] Ono, T. and Inoue, Y. (1983) FEBS Lett. 164, 255–260.
[21] Ono, T. and Inoue, Y. (1984) FEBS Lett. 166, 381–384.
[22] Åkerlund, H.E., Jansson, C. and Andersson, B. (1982) Biochim. Biophys. Acta 681, 1–10.
[23] Miyao, M. and Murata, N. (1985) FEBS Lett. 180, 303–308.
[24] Miyao, M. and Murata, N. (1989) Biochim. Biophys. Acta, 977, 315–321.
[25] Tsiotis, G., Walz, T., Spyridaki, A., Lustig, A., Engel, A. and Ghanotakis, D. (1996) J. Mol. Biol. 259, 241–248.
[26] Boekema, E.J, Hankamer, B., Bald, D., Kruip, J., Nield, J., Boonstra, A.F., Barber, J and Rögner, M (1995) Proc. Natl. Acad. Sci. USA 92, 175–179.
[27] Rögner, M, Dekker, J.P., Boekema, E.J. and Witt, H.T (1987) FEBS Lett. 219 (1) 207–211.
[28] Ford, R.C and Evans, M.C.W. (1983) FEBS Lett. 160, 159–164.
[29] Bassi, R., Machold, O. and Simpson, D. (1985) Carls. Res. Commun. 50(3), 145–162.
[30] Hayashi, H., Fujimura, Y., Mohanty, P.S. and Murata, N. (1993) Photosynth. Res. 36, 35–42.
[31] Bradford, M.M. (1976) Anal. Biochem. 72, 248–254.
[32] Laemmli, U.K. (1970) Nature (London) 227, 680–685.
[33] Wilkens, S. and Capaldi, R.A. (1992) Arch. Biochem. Biophys. 299 (1), 105–109.
[34] Hartvig, J.M. and Capaldi, R.A. (1991) Biochemistry 30, 1278–1284.
[35] Frank, J., Shimkin, B. and Dowse, H. (1981) Ultramicroscopy 6, 343–358.
[36] Van Heel, M. and Keegstra, W. (1981) Ultramicroscopy 7, 113–130.
[37] Harauz, G., Boekema, E. and Van Heel, M. (1988) Methods Enzymol. 164, 35–49.
[38] Van Heel, M. and Stöffler-Meilicke, M. (1985) EMBO J. 4(9), 2389–2395.
[39] Saxton, W.O. and Frank, J. (1977) Ultramicroscopy 2, 219–227.
[40] Lyon, M.K., Marr, K.M. and Furcinetti, P.S. (1993) J. Struct. Biol. 110, 133–140.
[41] Holzenburg, A., Shepherd, F.H. and Ford, R.C. (1994) Micron 25, 447–451.
[42] Nicholson, W.V., Shepherd, F.H., Rosenberg, M.F., Ford, R.C. and Holzenburg, A. (1996) Biochem. J. 315, 543–547.
[43] Holzenburg, A., Flint, T.D., Shepherd, F.H. and Ford, R.C. (1996) Micron 27, 121–127.
[44] Akey, C.W. and Edelstein, S.J. (1983) J. Mol. Biol. 163, 575–612.
[45] Frank, J., Zhu, J., Penczek, P., Li, Y., Srivastava, S., Verschoor, A., Radermacher, M., Grassucci, R., Lata, R.K. and Agrawal, R.K. (1995) Nature 376, 441–444.
[46] Stoylova, S., McPhie, P., Flint, T.D., Ford, R.C. and Holzenburg, A. (1996) in Photsynthesis: From Light to Biosphere; Proceeedings of the Xth International Conference (Mathis, P.. ed.), (3) pp. 333–386, Kluwer Academic, Dordrecht.
[47] Simpson, D.J. (1979) Carlsberg Res. Commun. 44, 305–336.
[48] Seibert., M., De Wit, M. and Staehelin, L.A. (1987) J. Cell. Biol. 105, 2257–2265.
[49] Rosenberg, M.F., Flint, T.D., Shepherd, F.H., Holzenburg, A. and Ford, R.C. (1996) In: Photosynthesis: Fom Light to Biosphere,. Vol III, pp. 369–372, Kluwer Academic, Dordrecht.
[50] Boekema, E.J., Boonstra, A.F., Dekker, J.P. and Rögner, M. (1994) J. Bioenerg. Biomemb. 26, 17–29.
[51] Nakazato, K., Toyoshima, C., Enami, I. and Inoue, Y. (1996) J. Mol. Biol. 257, 225–232.
[52] Dekker, J.P., Betts, S.D., Yocum, C.F. and Boekema, E.J. (1990) Biochemistry 29, 3220–3225.
[53] Bassi, R., Magaldi, A.G., Tognon, G., Giacometti, G.M. and Miller, K.R. (1989) Eur. J. Cell. Biol. 50, 84–93.